Quasiequilibrium Characterization of Mixed-Ion Coulomb Crystals

Kunihiro Okada,[1,*] Masanari Ichikawa,[1] Michiharu Wada,[2] and Hans A. Schuessler[3]
[1]*Department of Physics, Sophia University, 7-1 Kioicho, Chiyoda, Tokyo 102-8554, Japan*
[2]*RIKEN Nishina Center for Accelerator-Based Science, 2-1 Hirosawa, Wako, Saitama 351-0198, Japan*
[3]*Department of Physics, Texas A&M University, College Station, Texas 77843, USA*
(Received 24 February 2015; revised manuscript received 24 August 2015; published 23 November 2015)

We demonstrate the application of reliable methods to determine both the average micromotion energies and the number of sympathetically cooled ions (SCIs) embedded in mixed-ion Coulomb crystals in a linear Paul trap. The number of the SCIs and the micromotion energies for the observed mixed-ion crystals are determined by comparing experimentally obtained images with molecular-dynamics simulations, where the kinetic energies of SCIs trapped in rf fields are averaged in cold elastic collisions between the laser-cooled ions and virtual very light atoms. This combined method quickly achieves the quasiequilibrium state of large mixed Coulomb crystals with over 10^3 ions, regardless of the initial conditions, and shows that the previously used pseudopotential-based adiabatic approximations should be replaced by such molecular-dynamics simulations. In addition, a pattern-matching recognition procedure is introduced which objectively ascertains the number of ions. We also apply the presented characterization method to determine the reaction-rate constant between slow acetonitrile molecules and sympathetically cooled Ne^+ ions at a translational temperature lower than 10 K.

DOI: 10.1103/PhysRevApplied.4.054009

I. INTRODUCTION

Cold molecules and their ions open ways to investigate cold- and ultracold-ion chemistry and frequency metrology to study fundamental physics. In the latter research fields, the possibilities to test the time variation of the fine-structure constant (α) and the proton-electron mass ratio ($\beta = m_p/m_e$) were proposed [1]. Recently, precision vibrational spectroscopy of cold N_2^+ ions was also proposed for such an application [2]. With regard to ultracold-ion chemistry ion-atom hybrid traps were applied to study mesoscopic quantum systems and the association processes in mixed-ion-neutral systems [3,4]. The dynamics of ultracold collisions is a good example to the understand of underlying quantum effects, such as resonance scattering and tunneling. On the other hand, ion-molecule reactions at a temperature lower than 100 K are very important for astrochemistry [5]. Although there are many experimental studies for astrochemically relevant ion-molecule reactions [6–10], there is a still wide gap between the temperature required of the reaction rates in astrochemistry and the temperature of the available measurements [5]. Actually, most of such measurements were performed at the restricted range near room temperature [11]. Particularly, cold ion-polar molecule reactions have not been studied extensively in the laboratory owing to experimental difficulties, i.e., the condensation or sublimation of polar gases at low temperatures.

Recent experimental developments combining a linear Paul trap (LPT) for the generation of Coulomb crystals with a Stark velocity filter for producing cold polar molecules make it possible to measure cold ion-polar molecule reactions under ultrahigh-vacuum conditions [12]. In fact, we demonstrated reaction-rate measurements between sympathetically cooled N_2H^+ ions and velocity-selected polar molecules, namely CH_3CN [13]. Although in the above measurements the rotational temperatures of the molecules are not cooled, this general technique has the potential to enable a systematic study of cold ion-polar molecule reactions by combining a cryogenic ion trap and laser cooling with a cold polar molecule source [14].

In addition to the above applications, potential applications using multispecies Coulomb crystals will be explored [15]. Actually, many research groups are now actively pursuing investigations with Coulomb crystals containing highly charged ions or cold molecular ions for precision spectroscopy to study fundamental physics [16–19]. In these contexts, the development of novel methods for simulating and characterizing ion Coulomb crystals is important. For instance, the determination of the number of sympathetically cooled ions (SCIs) is required to obtain reaction-rate coefficients from rate measurements. However, it is difficult to directly measure the ion number by observing SCIs through laser-induced fluorescence (LIF). For small ion crystals, one can determine the absolute number of ions with single-ion resolution by comparing the observed LIF images of laser-cooled ions (LCIs) to the molecular-dynamics (MD) simulation images [20]. This characterization method is also useful for studies

*Corresponding author.
okada-k@sophia.ac.jp

in ion-atom hybrid traps. However, the method is tedious and not practical for large multispecies Coulomb crystals consisting of many thousands of ions.

The average kinetic energy of the target ions is also a key parameter for cold-ion chemistry, since it is directly linked to the binary collision energy under study. Although the micromotion energy of SCIs can be deduced from the width of the LIF spectra of LCIs, it is not direct information and requires an understanding of the line shape [21]. If the projection of LIF images of ion crystals including molecular ions is obtained, an average kinetic energy at an equilibrium position can be calculated by an analytical expression, which is derived by applying the adiabatic approximation and the zero-temperature limit to trapped ions [22]. However, for large Coulomb crystals the adiabatic expression deviates from an actual temperature because the ions normally diffuse in the ion crystal. Thus, it is necessary to determine it using a well-founded method. Although the micromotion effect was less important for some previous applications, it could become important for more recent applications such as the collision dynamics and the reactions between neutrals and the ions. In previous studies [23–25], the inclusion of time-dependent rf fields and radiation pressure forces into MD simulations have been performed to obtain micromotion energies. The results also pointed out that the effective kinetic energy depends critically on the shapes of Coulomb crystals [24].

In this paper, we propose an approach to determining both the average micromotion energy and the number of sympathetically cooled molecular ions by matching the photographically observed pictures of Coulomb crystals with simulated ones. The important fact is that in our method the usual special cooling and heating forces are not employed. Instead, we introduce cold elastic collisions (CEC) between laser-cooled ions and virtual very light atoms in the MD simulations in order to reproduce experimental LIF images of ion crystals [20]. It is well known that the CEC method provides a true cooling mechanism particularly when very light atoms are used. Apart from the number of ions, the fitting parameter to simulate the observed images is a physical one, namely the temperature of the virtual light atoms. Using this calculation approach, we can also determine the average position of each ion in a Coulomb crystal just by comparing experimental images and simulation images. In the present paper, we extended the CEC approach to obtain both average micromotion energies of the cooled ions and a reproduction of experimental LIF images.

The application of our method is done for both the large laser and sympathetically cooled ion crystals employed in cold-ion chemistry. The method quickly achieves the quasiequilibrium state of a large mixed Coulomb crystal consisting of over 10^3 ions with a reliable CEC-produced secular temperature regardless of initial conditions. For the precise determination of the absolute number of SCIs, we introduce a pattern-matching method by calculating the zero-mean normalized cross-correlation (ZNCC) values [26] to compare the observed LIF images with simulation images. In order to determine the relative number of SCIs, we use a simple method in which the volume of the nonfluorescent area of an ion Coulomb crystal is measured under the assumptions of cylindrical symmetry and a constant number density of the ions. By extensive simulations, this procedure is verified and a good correlation between the volume and the number of SCIs is confirmed under certain conditions. We also discuss the validity and the applicability of the conditions of the method. To demonstrate the present method, we apply it to large mixed Coulomb crystals to determine the reaction rates between cold CH_3CN and sympathetically cooled Ne^+ ions at a translational temperature lower than 10 K.

II. CALCULATION METHOD

We carry out extensive MD simulations to characterize ion Coulomb crystals in a LPT. The present simulation code builds on the previously developed codes [20,27]. In summary, ion trajectories and velocities of all the trapped ions are calculated by solving Newton's equations of motion under time-independent trapping forces by the radial pseudopotential and the axial harmonic potential while Coulomb forces between ions are considered. Moreover, cold elastic collisions between trapped ions and virtual very light atoms are introduced in order to reproduce the quasiequilibrium state of an ion Coulomb crystal. The reasons why this method works well to simulate the Coulomb crystals are described in a previous paper [20].

As pointed out in the Introduction, in the present simulations we extend the treatment of quasiequilibrium Coulomb crystals, which are obtained by our CEC approach [20], in order to obtain the micromotion energies by adding time-dependent rf fields and radiation pressure forces. The latter force is introduced to reproduce asymmetric structures of ion crystals when the cooling laser is irradiated from one side of the crystal. Our approach drastically reduces calculation steps in order to achieve the quasiequilibrium state of a large mixed-ion crystal under rf fields. This computing time reduction is important for the characterization of large mixed Coulomb crystals with over 10^3 ions. Actually, the MD simulations applying only radiation pressure forces will take a much longer time to achieve the quasiequilibrium state, if the initial conditions of the ions are randomly set.

As is usual, the sympathetic cooling effect is achieved by the Coulomb interactions between SCIs and LCIs. Then, we obtain the trajectories and velocities of all of the trapped ions as well as the simulation images of mixed Coulomb crystals. The important point of the present calculation method is that we can determine micromotion energies [24]

of the ion Coulomb crystals in the quasiequilibrium states in addition to the secular motion energies.

Since the computational time for calculating the ion-ion Coulomb repulsion forces is proportional to the square of the ion number, acceleration of the calculations is also necessary to simulate large Coulomb crystals consisting of over 10^3 ions. For this purpose, we introduce a special-purpose computer (GRAPE9, K&F Computing Research Co.) to accelerate the many-body simulations [28].

III. RESULTS AND DISCUSSIONS

A. Determination of the absolute number of ions

The observed LIF images of the Coulomb crystals in a linear Paul trap are well simulated by MD simulations. However, it is often difficult to select the best matching for the simulated image to the observed one. Although one may perform this determination process by comparing the detailed structures of the Coulomb crystals, it is desirable that the result is checked by an objective pattern-recognition method. For this purpose, the ZNCC value can be used to compare the observed image to simulation images [26].

Here, we demonstrated the pattern matching between the observed and simulated images by calculating the ZNCC values as described in Appendix A. An example of the LIF image of a large two-species Coulomb crystal composed of Ca^+ and $N_2{}^+$ ions is shown in Fig. 1(a). The bright part shows the laser-cooled crystallized Ca^+ ions, while the central dark area is caused by the presence of nitrogen molecular ions. Since the detailed experimental setup for the observation of two-species Coulomb crystals was described in our previous paper [13], we only briefly explain the imaging system to observe the LIF image of Ca^+ ions here. The LIF image of Ca^+ is observed by a cooled charge-coupled device camera with a ×10 magnification telecentric lens system. The accumulation period for imaging is typically 10 s. In order to increase the signal-to-noise ratio, we measure the dark charge-coupled device image and subtract it from the observed image.

The determination process of the ion number is as follows. First, we estimate the number of Ca^+ and $N_2{}^+$ ions by multiplying the volume of the ion distribution with the number density at 0 K [20], i.e.,

$$n_q = \frac{\epsilon_0 V_{\rm ac}^2}{m r_0^4 \Omega^2}, \tag{1}$$

where $V_{\rm ac}$ and Ω are the amplitude and angular frequency of the applied rf fields, and r_0 is the closest distance from the central axis of the trap to the rod electrodes. m and q are the mass and charge of an ion, respectively. ϵ_0 is the vacuum permittivity. The volume including Ca^+ and $N_2{}^+$ ions can be determined by measuring the dimension of the LIF image with the cylindrical symmetry of the ion distributions [13]. Then, we perform the MD simulations by applying the estimated ion numbers. The simulation results are compared to the observed LIF image and the number of each ion species is corrected for the next simulation. The above procedure is repeated in order to obtain a better matching between the observed and simulated images. Finally, we obtain simulation images which have similar structures and sizes with the observed image. Examples of these simulation images are shown in Fig. 1(a). Note that it is hard to identify which is the best matching image. In order to discriminate the difference,

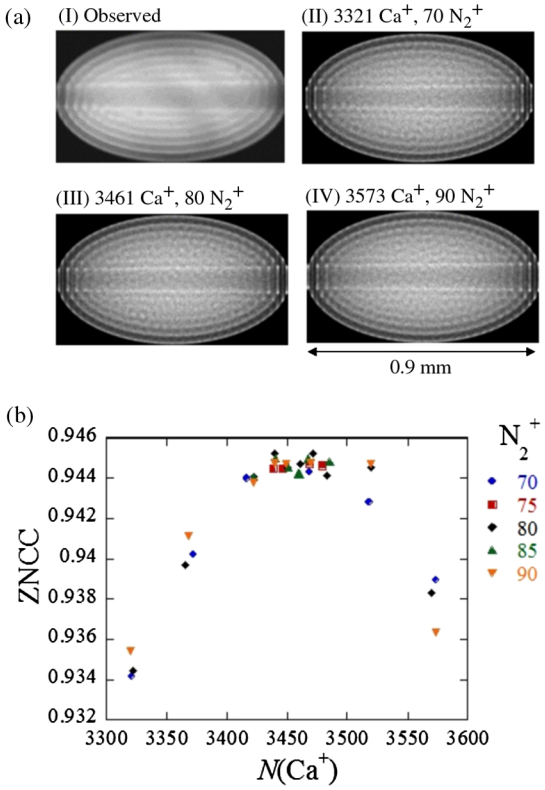

FIG. 1. (a) Comparison between the observed and MD simulation images. An observed LIF image of the two-component Coulomb crystal consisting of Ca^+ and $N_2{}^+$ ions (I) and MD simulation images for some different numbers of $N_2{}^+$ ions are also shown (II)–(IV). The driving rf frequency and the voltage of the linear Paul trap are $f_{\rm rf} = 4.875$ MHz and $V_{\rm ac} = 162.3$ V, respectively. The corresponding trap parameters for Ca^+ are $a = 0$ and $q = 0.068$, respectively. The static voltages applied to the end electrodes are set to $V_z = 4.0$ V. The geometrical factor (κ) along the trap axis is 0.28 [20]. The intensity and the detuning of the cooling laser are set to 3 mW/cm^2 and −10 MHz, respectively. In the MD simulations, the temperature of virtual very light atoms is set to 10 mK, which is chosen to obtain a large ZNCC value as much as possible. (b) A plot of the zero-mean normalized cross-correlation (ZNCC) values relating the simulation and the observed images for various sets of numbers of Ca^+ and $N_2{}^+$ ions. The different symbols show the ZNCC values for different numbers of $N_2{}^+$ ions. The maximum ZNCC value is obtained from where the numbers of Ca^+ and $N_2{}^+$ are 3460 (±30) and 80 (±10), respectively.

we calculate the ZNCC value for various sets of the numbers of Ca^+ and $N_2{}^+$ ions. The result is summarized in Fig. 1(b). Since the maximum value of the ZNCC is obtained for $N(N_2{}^+) = 80$ and the similar values are obtained for $70 \leq N(N_2{}^+) \leq 90$ in the range of $3430 \leq N(Ca^+) \leq 3490$, we determine the numbers of Ca^+ and $N_2{}^+$ to be 3460 (± 30) and 80 (± 10), respectively.

As demonstrated here, the present pattern-matching method can be used for the precise determination of the number of cold molecular ions embedded in Coulomb crystals. In other related experiments such as in cold-ion chemistry and molecular spectroscopy applying the resonance-enhanced multiphoton dissociation and ionization technique to sympathetically cooled molecular ions [4,29], the present method will reduce the uncertainty of the number of ions.

B. Relative number of SCIs embedded in ion crystals

For many applications, such as reaction-rate measurements between SCIs and neutral molecules [4,13,30], it is sufficient to know the relative number of ions in ion crystals. In our previous paper, we applied a simple method to determine the relative number of light SCIs embedded in ion crystals, and applied the method to the reaction-rate measurements between cold N_2H^+ and the velocity-selected CH_3CN [13]. In this particular case, the trapping potential for the molecular ions is deeper than that of Ca^+. Thus, the molecular ions are accumulated around the trap axis. The dark area in a two-component Coulomb crystal appears to be due to the existence of the molecular ions, as shown in Fig. 1(a). Since the number density of the cold molecular ions in the LPT has an almost constant value expressed by Eq. (1), the absolute number of ions is proportional to the volume of the dark area. We also assumed that the number of the SCIs between the curved and straight edge of the spheroid is very small on average and that the ion crystal has a cylindrical column distribution. Actually, we obtained a good correlation between the absolute numbers of the SCIs and the volumes calculated from the simulation images [13]. However, in Ref. [13] the proposed method was tested by MD simulations only in those special cases.

In the next section we present more extensive simulation results in order to analyze the correlation between the absolute number of SCIs and the volumes measured from the dimensions of the dark area in simulation images, including the case that the mass of the SCI is larger than that of the coolant ion. The process to obtain the dimensions of ion crystal images is explained in Appendixes B and C.

1. Ion-number dependence

First, we confirm the ion-number dependence of the correlation between the number of SCIs and the measured volume at a constant static voltage (V_z). As shown in Fig. 2, the number of Ca^+ is chosen to have two values of $N(Ca^+) = 4 \times 10^3$ and 3×10^2, and the correlation plots are obtained as a function of the number of N_2H^+ ions. The value of R in the graph indicates the correlation coefficient which has the optimum value of 1. We have confirmed that a good correlation of practically 1 between the number of SCIs and the measured volume is obtained for this range of the total number of ions.

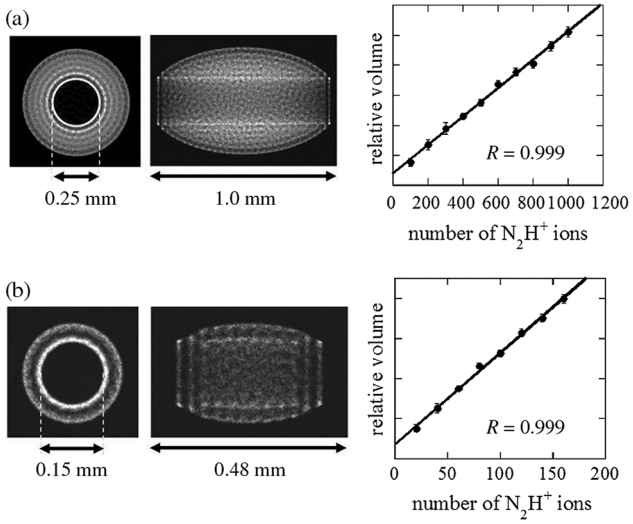

FIG. 2. The left simulation images show the cross-section and the side-view images in different sizes of two-component Coulomb crystals consisting of Ca^+ and N_2H^+ ions. (a) $N(Ca^+) = 4 \times 10^3$, $N(N_2H^+) = 1 \times 10^3$, (b) $N(Ca^+) = 3 \times 10^2$, $N(N_2H^+) = 1.6 \times 10^2$. The right graphs are plots of the volume of the dark area as a function of the number of N_2H^+ ions. The value of R in the graph indicates the correlation coefficient. The simulation parameters are the same as in Fig. 1.

As shown in Fig. 3, this good correlation close to 1 is maintained even if the aspect ratio (a/b with a and b being the major and minor axes of the spheroid) of the spheroidal Ca crystals are taken between 5.0 to 0.68 (see Fig. 5). We also check that a good correlation is obtained for different mass numbers of the SCIs (M_s) between 17 and 39.

2. Peripheral distribution of SCIs

For ions heavier than Ca^+, the SCIs are distributed outside the Ca^+ crystals. We find that the volume of the dark area of the LIF in the crystals is also correlated with the absolute number of the SCIs with the mass of $41 \leq M_s \leq 78$ by applying a relatively high V_z, i.e., the aspect ratio of the crystal is $a/b < 5.0$. Actually, the volume of the dark area is calculated by substituting the elliptic parameters obtained from the simulation image of Ca^+ into Eq. (C3).

Examples of the simulation results are shown in Fig. 4. As expected, the smaller the mass number of SCIs, the higher the correlation coefficient that is obtained. Since the

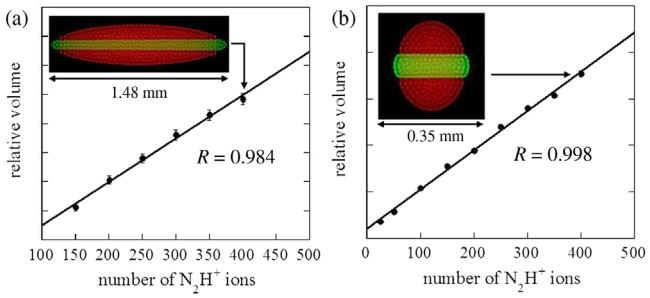

FIG. 3. The correlation between the volume of the dark area and the ion number at different static voltages. The number of Ca^+ ions is set to 2×10^3. The red and green areas in the inset side-view images show Ca^+ ions and N_2H^+, respectively. The other simulation parameters are the same as in Fig. 1 except for V_z. (a) $V_z = 1.5$ V and (b) $V_z = 8.0$ V

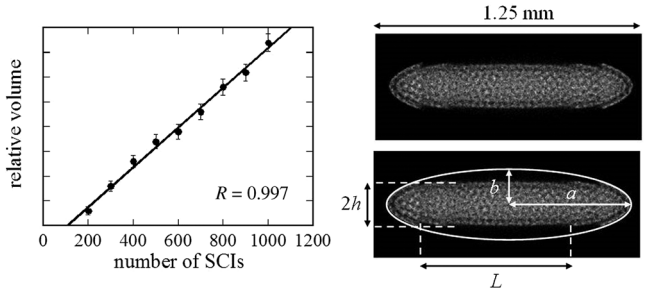

FIG. 5. The correlation plot between the volume of the dark area and the number of SCIs with $M_s = 41$ for $a/b \sim 3.45$. The numbers of Ca^+ is set to 1×10^3 and the simulation parameters are the same as in Fig. 1 except for $V_z = 2.0$ V. The correlation coefficient is $R = 0.997$. The right side-view image explain the parameters to calculate the volume of the distributed SCIs.

trapping force for heavier ions becomes weaker, the degree of the shape change is smaller as the mass of SCI increases. As shown in Fig. 4, the dark area outside the Ca^+ crystal seems to be not directly linked with the distribution of SCIs with $M_s = 70$. However, the calculated volume of the dark area, which is obtained by assuming the spheroidal shape of the two-species Coulomb crystal, has a good correlation to the number of SCIs in the range $200 \leq N_s \leq 2000$.

For larger a/b, we have tested whether there is the correlation between the dark area and the number of SCIs with $M_s = 41$. In this case, the volume of the dark region is calculated by

$$V'_{\text{outer}} = \frac{4}{3}\pi ab^2 - \pi h^2 L - 2\pi b^2\left(\frac{2}{3}a - L + \frac{L^3}{3a^2}\right), \quad (2)$$

where L and h are the length and the height of the cylindrical distribution of LCIs (Fig. 5). As shown in Fig. 5, a good correlation is obtained also in this particular case. According to the simulation results so far, we can therefore expect to obtain a good correlation for heavier SCIs. However, we expect that there is an upper limit of the mass number and a lower limit of the number of SCIs in order to obtain a good correlation in a specific simulation condition.

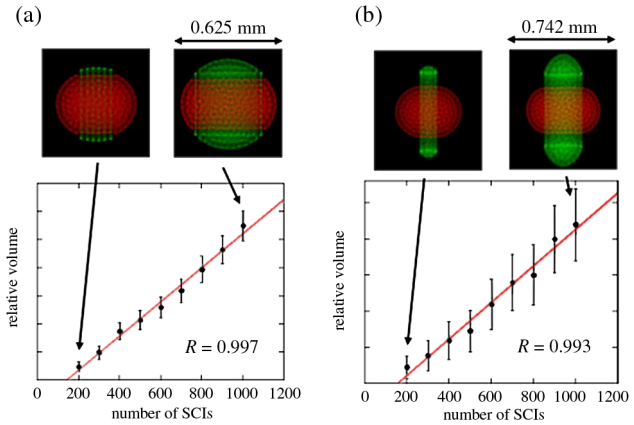

FIG. 4. The correlation between the volume of the dark area and the number of SCIs with different mass numbers. The red and green areas in the upper simulation images show Ca^+ ions and SCIs with $M_s = 44$ (a) and $M_s = 70$ (b), respectively. The number of Ca^+ ions is set to 1×10^3 and the simulation parameters are the same as in Fig. 1 except for $V_z = 6.0$ V.

C. Determination of micromotion energies

As previously mentioned, the micromotion energy is an important parameter in applications of cold-ion chemistry and precision spectroscopy of atomic and molecular ions [12,13,22]. In particular, the reliable determination of the micromotion energies in large-ion crystals containing over thousands of ions has been an unsettled problem. Here we demonstrate a method to determine it.

Figure 6(a) shows the simulation images of a two-component Coulomb crystal consisting of 4×10^3 Ca^+ and 2.5×10^2 N_2H^+ ions. Since the rf fields are applied in the calculations, it is possible to obtain the average micromotion energy of each ion in the ion crystal. Plots of the micromotion energy as a function of the number of N_2H^+ are shown in Fig. 6(b), where these micromotion energies are labeled by "MD" in the graph. The unit of the energy is expressed in kelvin. We also plot for comparison the energies calculated by Eqs. (C5), (C6), and (C7) of Appendix C. It is clear that the adiabatic equations of Eqs. (C5) and (C6) always underestimate (overestimate) the energy of the outer (inner) ions in spheroidal ion crystals and are not correct. On the other hand, Eq. (C7), which is derived by the approximation of the column distribution of SCIs, reproduces well the results by MD simulations.

As shown in Fig. 7, the difference becomes large when applying higher static voltages along the trap axis. It is noted that the average micromotion energy of SCIs can be controlled by changing an axial voltage (V_z), as pointed out in Ref. [24]. In this case, the tuning range of the micromotion energy is $1\ \text{K} < T < 6\ \text{K}$.

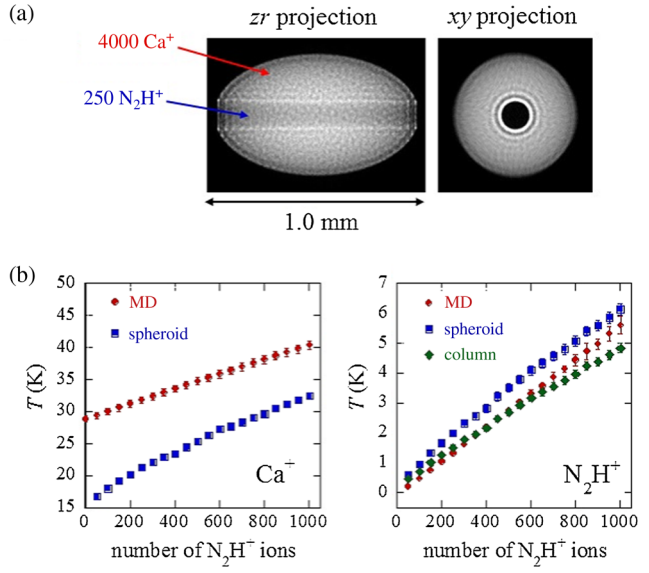

FIG. 6. (a) Simulation images of a two-component Coulomb crystal consisting of 4×10^3 Ca^+ and 2.5×10^2 N_2H^+ ions under rf fields. (b) Plots of the micromotion energy as a function of the number of N_2H^+: left, Ca^+; right, N_2H^+. The red solid circles show the results by MD simulations. The blue solid squares show the micromotion energies obtained by adiabatic calculations using Eqs. (C5) and (C6). The green solid diamonds show the results by Eq. (C7).

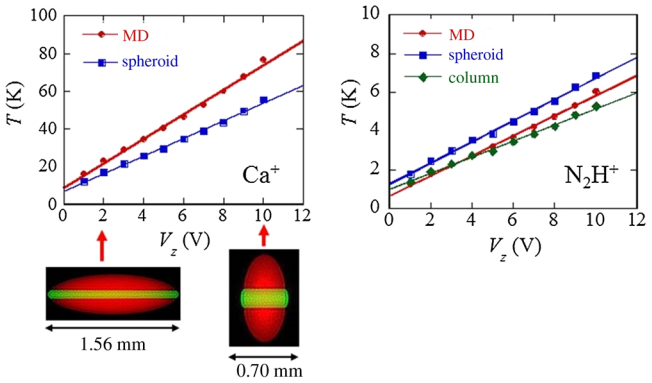

FIG. 7. Axial voltage dependence of the micromotion energies. The ion crystal consists of 4×10^3 Ca^+ and 5×10^2 N_2H^+ ions. The difference between the simulation and the analytical results increases as V_z increases.

Figures 8 show plots of the average micromotion energies as a function of the temperature of the virtual very light atoms (T_{sec}) in the collision cooling method. The results suggest that the micromotion energy of SCIs has a small dependence on the secular motion temperature of the ions. However, the dependence is very small or negligible, at least for $T_{sec} \leq 15$ mK.

D. Application to reaction-rate measurements

As a first application of our improved method, we characterize experimentally observed two-species

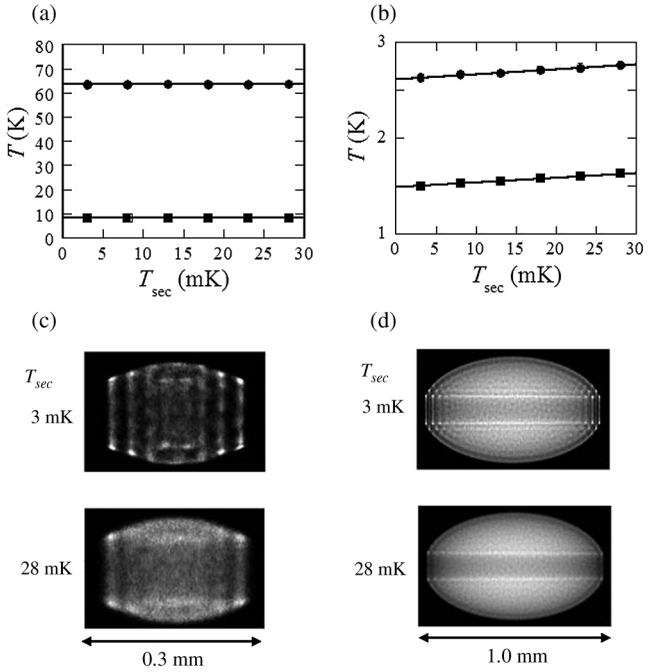

FIG. 8. (a) A plot of an average micromotion energy of Ca^+ as a function of the temperature of the virtual very light atoms in the collision cooling method. The solid circles and squares indicate the average of 4×10^3 Ca^+ ions and 1×10^2 Ca^+ ions, respectively. The micromotion energy is expressed in kelvin. (b) A plot of an average micromotion energy of N_2H^+. The solid circles and squares indicate the average of 2.5×10^2 N_2H^+ in 4×10^3 Ca^+ ions and 5×10^1 N_2H^+ in 1×10^2 Ca^+ ions, respectively. The corresponding simulation images are shown in (c) and (d).

Coulomb crystals consisting of Ca^+ and Ne^+, and determine the reaction-rate constant between slow acetonitrile molecules (CH_3CN) and sympathetically cooled Ne^+. Velocity-selected CH_3CN molecules are produced by a Stark velocity filter, which was previously described [13]. The number density of slow CH_3CN at the trap center is determined separately. It is determined to be $8.8(2.3) \times 10^4$ cm^{-3} in the present measurement. The translational temperature ($T_{1D} \sim 6.5$ K) is also estimated by combining the result of the time-of-flight measurement to the numerical simulations of the velocity filtering of CH_3CN [13].

The detail of the ion trap was described in our previous paper [13]. Here, we briefly summarize it as follows. The base pressure of the vacuum chamber enclosing a linear Paul trap is evacuated to be less than 10^{-8} Pa. Since the base plate of the linear trap is cooled by a liquid-nitrogen baffle, the main residual gas in the trap regions is expected to be H_2. In fact, this cryogenic linear trap is indispensable to avoiding undesirable reactions between cold ions and stray polar molecules, which can possibly leak from upstream of the Stark velocity filter. For the sympathetic laser cooling of molecular ions, Ca^+ ions are produced and trapped by the laser-ablation method while suitable ejection rf voltages at the secular motion frequencies for unwanted ions are applied to the trap electrodes during the trapping

and cooling processes in order to remove impurity ions [30]. Before starting the reaction-rate measurement, we confirm that there are no dark areas in the LIF images of the Ca^+ Coulomb crystals. We equip the setup with an electron gun for producing Ne^+ ions by electron-impact ionization. Neon gas of about 1×10^{-6} Pa is introduced into the vacuum chamber during the production. Although a small fraction of $H_2{}^+$ ions might be produced, such ions cannot be sympathetically cooed by laser-cooled Ca^+ ions due to the large mass difference between Ca^+ and $H_2{}^+$.

Figure 9(a) shows snapshots of the LIF images at certain reaction times. The dark area caused by Ne^+ ions progressively decreases with increasing reaction time due to the progress of the $CH_3CN + Ne^+ \rightarrow$ products reactions. The decay curve of the relative number of Ne^+ ions is also shown in Fig. 9(b). Each data point is obtained from the volume of the dark area in the LIF images, as explained in Sec. III B. In the present experiment, a small fraction of the dark inner core is left at the end. As shown in Fig. 9(c), there are three possible reaction paths. Since the mass of NeH^+ is smaller than that of Ca^+, the observed residual ions in the dark middle of the ion crystal are with high likelihood NeH^+ ions. A further experimental study is needed to confirm the residual ions by measuring the mass spectra of extracted ions from the Coulomb crystal. This could be done by a newly developed technique [32].

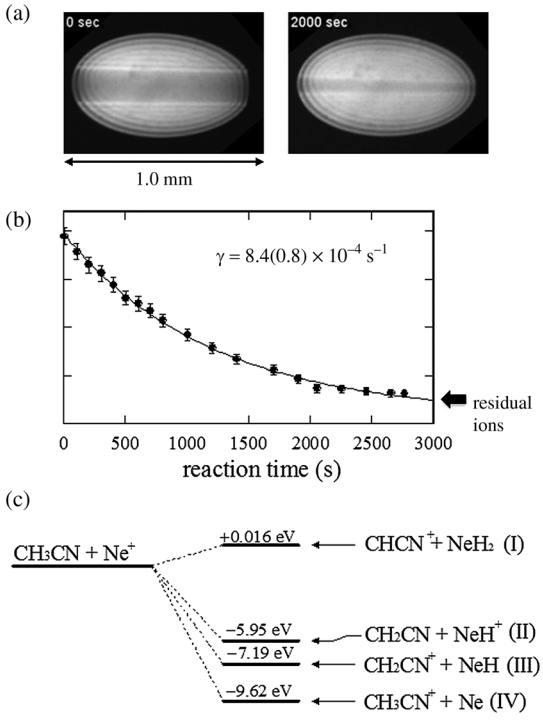

FIG. 9. (a) Snapshots of the LIF images from two-component Coulomb crystals including Ca^+ and Ne^+ during the $CH_3CN + Ne^+ \rightarrow$ products reactions. The reaction time is indicated in each image. (b) A plot of the relative number of Ne^+ ions as a function of the reaction time in $CH_3CN + Ne^+ \rightarrow$ products reactions. (c) Energy diagram of the Ne^+-CH_3CN reaction system calculated by the quantum chemical calculation packages (Gaussian 03) [31]. The geometry optimization of the molecular ions and calculations of the zero-point energies are performed by B3LYP/6-31G(d). The ground-state energies are calculated using B3LYP/6-311 + $(3df, 3pd)$ in the optimized geometries.

In order to extract the reaction rate of $CH_3CN + Ne^+ \rightarrow$ products, we perform a least-squares fit of the exponential function with a background term to the data of Fig. 9(b). The reaction rate is determined to be $\gamma = 8.4(0.8) \times 10^{-4}\,s^{-1}$. Data points up to 46 min in reaction time are used to obtain the reaction rate. Note that the decay rate of Ne^+ without slow CH_3CN is evaluated to be $< 10^{-4}$ s^{-1} by separate measurements.

The average reaction temperature T_{avg} is estimated by the following equation:

$$T_{avg} = T_{ion}\frac{\mu}{M_{ion}} + T_{PM}\frac{\mu}{M_{PM}}, \tag{3}$$

where T_{ion} and T_{PM} are the average temperatures of the ions and the polar molecules, respectively. $\mu = M_{ion}M_{PM}/(M_{ion} + M_{PM})$ is the reduced mass of the ion and the molecule. In order to determine the average reaction temperature, we perform the MD simulations of large two-component Coulomb crystals containing Ca^+ and Ne^+. By comparison between the observed images shown in Fig. 9(a) and the simulation images, the number of Ca^+ is determined to be $4.25(0.25) \times 10^3$ ions [Fig. 10(a)]. In Fig. 10(b), the averaged micromotion energies of the Ne^+ ions are plotted as a function of the

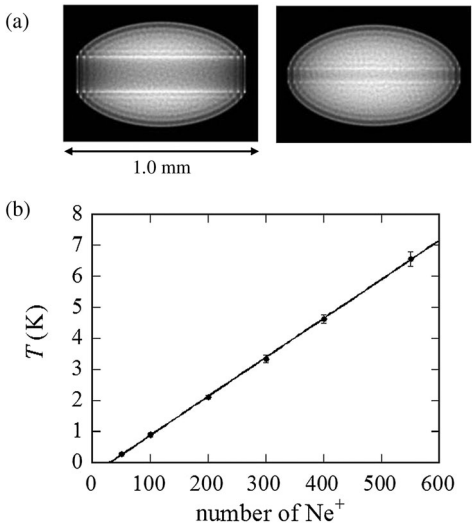

FIG. 10. (a) Corresponding simulation images to Fig. 9(a). The number of Ca^+ is $4.25(0.25) \times 10^3$. The numbers of Ne^+ is 550 and 50, respectively. The temperature of virtual very light atoms is set to 12 mK. (b) A plot of average micromotion energy of Ne^+ obtained by the MD simulations. The other calculation parameters are the same as the experimental conditions. The micromotion energy decreases from 6.6 to 0.3 K when the number of Ne^+ decreases from 550 to 50.

number of Ne^+. The micromotion energy decreases from 6.6 to 0.3 K when the number of Ne^+ decreases from 550 to 50. However, the energy is not sensitive to the difference of the number of Ca^+ ions. The average reaction temperature calculated by Eq. (3) changes with the number of Ne^+ ions from 6.5 to 2.3 K in the present experiment. It is to be noted that the simulation results imply that the smaller the number of Ne^+ yields, the more accurate the reaction temperature.

As described in our previous paper [13], the number density n and the translational temperature T_{1D} of the velocity-selected CH_3CN was determined by a separate measurement. In the present experiment, $n = 8.8(2.3) \times 10^4$ cm^{-3} and $T_{1D} = 6.5$ K are obtained. Thus, the preliminary result of the reaction-rate constant k is obtained by $k = \gamma/n$, resulting in $9.5(2.6) \times 10^{-9}$ cm^3 s^{-1} at the translational temperature between 6.5–2.3 K. The error is caused by the uncertainty of the number density of the CH_3CN molecules and the statistical error. It should be noted that the systematic errors including a variation of the reaction temperature and the background decay of Ne^+ are not considered in the present value. For comparison, we estimate the ion-dipole capture rate using the trajectory scaling formula [33]. This formula is obtained by parametrizing the results of trajectory simulations of an ion-dipole system, where the rotational and translational dynamics are considered. Using this formula, the capture rate of the CH_3CN-Ne^+ system is estimated to be $k_{ts} = 2.9$–4.8×10^{-8} cm^3 s^{-1} at 6.5–2.3 K. Since the formula yields the upper limit of ion-dipole capture rates under the assumed conditions, the present result is consistent with the calculated values. One of the possible reasons for the difference between the present experimental result and the capture rates is the difference of rotational temperatures. In the present experiment, the rotational temperature of slow CH_3CH is evaluated to be about 100 K from the rotational state distribution obtained by numerical simulations [13]. Since in the present experiment sufficient rotational cooling of CH_3CN is not realized, further studies are needed to test the scaling formula.

IV. SUMMARY AND OUTLOOK

In summary, we perform molecular-dynamics simulations for quasiequilibrium ion crystals, which are obtained by cold elastic collisions between laser-cooled ions and virtual very light atoms in order to characterize two-component Coulomb crystals. We demonstrate determining the absolute number of ions in large ion Coulomb crystals using the pattern-matching method by calculating the ZNCC values between experimental and simulated images of the ion crystal. The method yields an objective result in the determination process.

Then we propose a simple method to determine the relative number of SCIs by LIF images of two-component Coulomb crystals. Our extensive simulations show that good correlations exist between the calculated volume of the dark area due to the SCIs in the LIF images and the absolute number. The method can even be applied to heavier ions than the laser-cooled ions, where in this case the SCIs are pushed to the outside of the coolant ions in ion crystals.

The time-averaged kinetic energies of the ions are calculated. The novel key point of the present method is that the MD simulations are performed in time-dependent quadrupole fields while simultaneously elastic collisions between LCIs and virtual very light atoms are applied. The collision cooling method reproduces realistic conditions of an experimental ion Coulomb crystal [20]. Thus, by adding the rf fields in the simulation, we can obtain reliable micromotion energies of ion Coulomb crystals.

Finally, we apply the present characterization methods to the determination of the reaction-rate constant between velocity-selected CH_3CN and sympathetically cooled Ne^+ at a translational temperature lower than 10 K. The sequential LIF images of the two-component Coulomb crystals during the reaction are used to extract the relative number of Ne^+ ions by the described method. The average reaction temperature is deduced from the known kinetic temperature of the slow CH_3CN molecules and the micromotion energies of sympathetically cooled Ne^+ ions, which is obtained by a reliable method.

The present characterization methods for ion Coulomb crystals is applicable to other research fields, such as precision spectroscopy of sympathetically cooled highly charged ions (HCIs) and molecular ions, in addition to cold-ion chemistry. Since the sympathetic cooling in ion Coulomb crystals in linear Paul traps is a promising method to generate cold molecular ions or cold HCIs for studying the time variation of fundamental physical constants [2,17], the characterization of sympathetically cooled HCIs and molecular ions is indispensable. In particular, the micromotion energy and the spatial distribution of the SCIs are the key parameters for extremely accurate spectroscopy. In the near future, we will perform a systematic simulation study of sympathetic cooling of HCIs for this purpose [19].

ACKNOWLEDGMENTS

This work is financially supported in part by a Grant-in-Aid for Young Scientists (A) from the Ministry of Education, Culture, Sports, Science and Technology (MEXT), the Robert A. Welch Foundation under Grant No. A1546, and the Matsuo Foundation.

APPENDIX A: PATTERN-MATCHING METHOD

The zero-mean normalized cross-correlation (ZNCC) can be written as

$$\mathrm{ZNCC} = \frac{\sum (I_{ij} - \bar{I})(T_{ij} - \bar{T})}{\sqrt{\sum (I_{ij} - \bar{I})^2} \sqrt{\sum (T_{ij} - \bar{T})^2}}, \quad \text{(A1)}$$

which takes a value between −1 and +1 [26]. I_{ij} and T_{ij} are pixel values of the observed and simulated images, respectively. $\bar{I}$ and $\bar{T}$ are the mean intensity values. Since the matching value (ZNCC) is robust against linear brightness variations between the observed and template images, it is useful for the present purpose.

APPENDIX B: DETERMINATION OF THE BOUNDARY OF A TWO-COMPONENT ION COULOMB CRYSTAL

We consider the case of a two-component Coulomb crystal consisting of the LCIs and the lighter SCIs. An example simulation image of the two-component Coulomb crystal is shown in Fig. 11(a). The length of the axial distribution of the SCIs is almost constant when there are sufficient numbers so that the ions extend to both ends of the Ca^+ crystal. As mentioned in Sec. III B, we assume that the number of the SCIs between the curved and straight edge of the spheroid is very small on average and that the ion crystal has a cylindrical column distribution. Thus, the volume of the dark area is proportional to the square of the column radius. In order to determine this radius, the projection of the image along the trap axis (z) is taken. Then we obtain the projection profile of the image as a function of the radial coordinate (r), as shown in Fig. 11(b). The column diameter ($2h$) is taken as a distance between the two nearest peaks from the trap axis.

APPENDIX C: ANALYTICAL EXPRESSIONS OF MICROMOTION ENERGIES

According to the adiabatic approximation for a single trapped ion in a linear Paul trap, the average micromotion energy can be expressed as

$$E_m(r) = \alpha q^2 r^2, \tag{C1}$$

$$\alpha = \frac{V_{\mathrm{ac}}^2}{m r_0^4 \Omega^2}. \tag{C2}$$

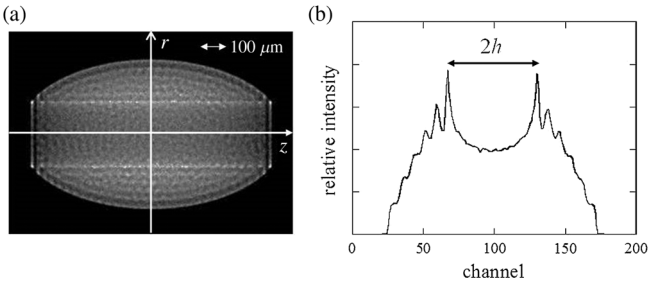

FIG. 11. (a) The simulation image of a two-component Coulomb crystal consisting of 4×10^3 Ca^+ and 1×10^3 N_2H^+ ions. The dark area is caused by the existence of the SCIs. The simulation parameters are the same as in Fig. 1. (b) Projection of the image (a) along the z axis. The column diameter of the dark area is taken as a distance between two nearest peaks from the center, i.e., $2h$.

We consider the case that the two-component Coulomb crystals are distributed in a spheroid with a constant number density. Generally, the lighter ions are subjected to a stronger trapping force and gather near the trap axis, when the ions are cooled. In experiments it is possible to discriminate the boundary of the two ion species from the observed LIF images [see Figs. 1(a) and 5]. Therefore, the volume of the outer part of the spheroid is given by

$$V_{\mathrm{outer}} = \frac{2\pi a (b-h)^2 (2b+h)}{3b}, \tag{C3}$$

where a and b are the major and minor axes, and h is a distance between the trap axis and the boundary of the different ion species (see Fig. 12). The volume of the inner part is

$$V_{\mathrm{inner}} = \frac{2}{3}\pi a b h \left(3 - \frac{h^2}{b^2}\right). \tag{C4}$$

In the case of the Coulomb crystals consisting of LCIs and lighter SCIs, such as Ca^+ and N_2H^+, the distribution of the inner molecular ions can be approximated in a cylindrical shape. If the few SCIs between the curved and straight edge of the spheroid are ignored, the volume is approximated by $2\pi a h^2$.

For the outer ions the average micromotion energy can be calculated as follows:

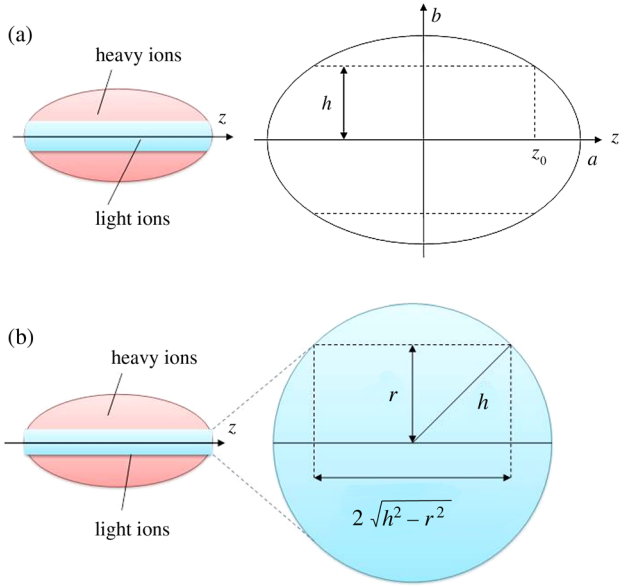

FIG. 12. (a) The spheroidal ion distribution of a two-component Coulomb crystal. The right figure shows the definition of the parameters related to the spheroid. (b) The approximated cylindrical ion distribution of the inner light ions. The figures on the right show the cross section of the inner ions.

$$E_{\text{outer}} = 2\int_h^b n_q E_m(r) S(r) dr/(n_q V_{\text{outer}}) = \frac{\alpha q^2}{5}\left\{\frac{2b^2(b+2h)}{2b+h} + 3h^2\right\}, \quad \text{(C5)}$$

where $S(r)$ is the cross section of the spheroid crystal at distance r from the trap axis, and n_q is the number density of the ions. Similar expressions can be obtained for the inner ions (E_{inner}) and the cylindrical distribution ($E_{\text{cylindrical}}$), that is,

$$E_{\text{inner}} = \frac{\alpha q^2 h^2(5b^2 - 3h^2)}{5(3b^2 - h^2)}, \quad \text{(C6)}$$

$$E_{\text{cylindrical}} = \frac{1}{4}\alpha q^2 h^2. \quad \text{(C7)}$$

These expressions can be used to estimate the average micromotion energies of two-component Coulomb crystals in a linear Paul trap. We compare the estimated values with the simulation results in Sec. III C.

[1] S. Schiller and V. Korobov, Tests of time independence of the electron and nuclear masses with ultracold molecules, Phys. Rev. A **71**, 032505 (2005).

[2] M. Kajita, G. Gopakumar, M. Abe, M. Hada, and M. Keller, Test of m_p/m_e changes using vibrational transitions in N_2^+, Phys. Rev. A **89**, 032509 (2014).

[3] C. Zipkes, S. Palzer, C. Sias, and M. Köhl, A trapped single ion inside a Bose-Einstein condensate, Nature (London) **464**, 388 (2010).

[4] F. H. J. Hall, M. Aymar, N. Bouloufa-Maafa, O. Dulieu, and S. Willitsch, Light-Assisted Ion-Neutral Reactive Processes in the Cold Regime: Radiative Molecule Formation versus Charge Exchange, Phys. Rev. Lett. **107**, 243202 (2011).

[5] V. Wakelam, I. W. M. Smith, E. Herbst, J. Troe, W. Geppert, H. Linnartz, K. Öberg, E. Roueff, M. Agundez, P. Pernot, H. M. Cuppen, J. C. Loison, and D. Talbi, Reaction networks for interstellar chemical modelling: Improvements and challenges, Space Sci. Rev. **156**, 13 (2010).

[6] B. R. Rowe, G. Dupeyrat, J. B. Marquette, and P. Gaucherel, Study of the reactions $N_2^+ + 2N_2 \rightarrow N_4^+ + N_2$ and $O_2^+ + 2O_2 \rightarrow O_4^+ + O_2$ from 20 to 160 K by the CRESU technique, J. Chem. Phys. **80**, 4915 (1984).

[7] B. R. Rowe and J. B. Marquette, CRESU studies of ion/molecule reactions, Int. J. Mass Spectrom. Ion Process. **80**, 239 (1987).

[8] D. Gerlich, Ion-neutral collisions in a 22-pole trap at very low energies, Phys. Scr. **T59**, 256 (1995).

[9] D. Gerlich and G. Borodi, Buffer gas cooling of polyatomic ions in rf multi-electrode traps, Faraday Discuss. **142**, 57 (2009).

[10] I. W. M. Smith, Laboratory astrochemistry: Gas-phase processes, Annu. Rev. Astron. Astrophys. **49**, 29 (2011).

[11] J. Woodall, M. Agundez, A. J. Markwick-Kemper, and T. J. Millar, The UMIST database for astrochemistry 2006, Astron. Astrophys. **466**, 1197 (2007).

[12] S. Willitsch, M. T. Bell, A. D. Gingell, S. R. Procter, and T. P. Softley, Cold Reactive Collisions between Laser-Cooled Ions and Velocity-Selected Neutral Molecules, Phys. Rev. Lett. **100**, 043203 (2008).

[13] K. Okada, T. Suganuma, T. Furukawa, T. Takayanagi, M. Wada, and H. A. Schuessler, Cold ion-polar-molecule reactions studied with a combined Stark-velocity-filterion-trap apparatus, Phys. Rev. A **87**, 043427 (2013).

[14] L. D. van Buuren, C. Sommer, M. Motsch, S. Pohle, M. Schenk, J. Bayerl, P. W. H. Pinkse, and G. Rempe, Electrostatic Extraction of Cold Molecules from a Cryogenic Reservoir, Phys. Rev. Lett. **102**, 033001 (2009).

[15] M. Drewsen, Ion Coulomb crystals, Physica (Amsterdam) **460B**, 105 (2015).

[16] S. Willitsch, Coulomb-crystallized molecular ions in traps: Methods, applications, prospects, Int. Rev. Phys. Chem. **31**, 175 (2012).

[17] V. A. Dzuba, V. V. Flambaum, and Hidetoshi Katori, Optical clock sensitive to variations of the fine-structure constant based on the Ho^{14+} ion, Phys. Rev. A **91**, 022119 (2015).

[18] L. Schmöger, O. O. Versolato, M. Schwarz, M. Kohnen, A. Windberger, B. Piest, S. Feuchtenbeiner, J. Pedregosa-Gutierrez, T. Leopold, P. Micke, A. K. Hansen, T. M. Baumann, M. Drewsen, J. Ullrich, P. O. Schmidt, and J. R. Crespo López-Urrutia, Coulomb crystallization of highly charged ions, Science **347**, 1233 (2015).

[19] K. Okada, M. Ichikawa, and M. Wada, *Proceedings of the 6th International Conference on Trapped Charged Particles and Fundamental Physics (TCP 2014), Takamatsu, Japan*, (Springer International Publishing, Switzerland, 2015).

[20] K. Okada, M. Wada, T. Takayanagi, S. Ohtani, and H. A. Schuessler, Characterization of ion Coulomb crystals in a linear Paul trap, Phys. Rev. A **81**, 013420 (2010).

[21] V. L. Ryjkov, X. Z. Zhao, and H. A. Schuessler, Sympathetic cooling of fullerene ions by laser-cooled Mg^+ ions in a linear rf trap, Phys. Rev. A **74**, 023401 (2006).

[22] A. K. Hansen, O. O. Versolato, Ł. Klosowski, S. B. Kristensen, A. Gingell, M. Schwarz, A. Windberger, J. Ullrich, J. R. Crespo López-Urrutia, and M. Drewsen, Efficient rotational cooling of Coulomb-crystallized molecular ions by a helium buffer gas, Nature (London) **508**, 76 (2014).

[23] C. B. Zhang, D. Offenberg, B. Roth, M. A. Wilson, and S. Schiller, Molecular-dynamics simulations of cold single-species and multispecies ion ensembles in a linear Paul trap, Phys. Rev. A **76**, 012719 (2007).

[24] T. M. Bell, A. D. Gingell, J. M. Oldham, T. P. Softley, and S. Willitsch, Ion-molecule chemistry at very low temperatures: Cold chemical reactions between Coulomb-crystallized ions and velocity-selected neutral molecules, Faraday Discuss. **142**, 73 (2009).

[25] F. H. J. Hall and S. Willitsch, Millikelvin Reactive Collisions between Sympathetically Cooled Molecular Ions and Laser-Cooled Atoms in an Ion-Atom Hybrid Trap, Phys. Rev. Lett. **109**, 233202 (2012).

[26] G. J. Vanderburg and A. Rosenfeld, Two stage template matching, IEEE Trans. Comput. **C-26**, 384 (1977).

[27] K. Okada, K. Yasuda, T. Takayanagi, M. Wada, H. A. Schuessler, and S. Ohtani, Crystallization of Ca^+ ions in a linear rf octupole ion trap, Phys. Rev. A **75**, 033409 (2007).

[28] A. Kawai, T. Fukushige, J. Makino, and M. Taiji, GRAPE-5: A Special-Purpose Computer for *N*-Body Simulations, Publ. Astron. Soc. Jpn. **52**, 659 (2000).

[29] X. Tong, A. H. Winney, and S. Willitsch, Sympathetic Cooling of Molecular Ions in Selected Rotational and Vibrational States Produced by Threshold Photoionization, Phys. Rev. Lett. **105**, 143001 (2010).

[30] N. Kimura, K. Okada, T. Takayanagi, M. Wada, S. Ohtani, and H. A. Schuessler, Sympathetic crystallization of CaH^+ produced by a laser-induced reaction, Phys. Rev. A **83**, 033422 (2011).

[31] The reaction enthalpy at 0 K is calculated using theGaussian 03 program package [M. J. Frisch *et al.*, Gaussian 03 Revision B.01 (Gaussian Inc. Pittsburgh, PA, 2003)].

[32] N. Deb, L. L. Pollum, A. D. Smith, M. Keller, C. J. Rennick, B. R. Heazlewood, and T. P. Softley, Coulomb crystal mass spectrometry in a digital ion trap, Phys. Rev. A **91**, 033408 (2015).

[33] T. Su and W. J. Chesnavich, Parameterization of the ion-polar molecule collision rate constant by trajectory calculations, J. Chem. Phys. **76**, 5183 (1982).